

PAG neurons encode a simplified action-selective signal during aggression

Annegret L. Falkner^{1,2*}, Dongyu Wei⁴, Anjeli Song³, Li W. Watsek², Irene Chen², James E. Feng², Dayu Lin^{2,4,5}

¹ Princeton Neuroscience Institute, Princeton, NJ 08540, U.S.A

² Neuroscience Institute, New York University School of Medicine, New York, NY 10016, U.S.A.

³ Boston University School of Medicine, Boston, MA 02118, U.S.A.

⁴ Department of Psychiatry, New York University School of Medicine, New York, NY 10016, U.S.A.

⁵ Center for Neural Science, New York University, New York, NY 10003, U.S.A.

*Correspondence: afalkner@princeton.edu

1 **Summary**

2 While the ventromedial hypothalamus, ventrolateral area (VMHvl) is now well established as a
3 critical locus for the generation of conspecific aggression, its role is complex, with populations of
4 neurons responding during the motivational, sensory, and action phases of aggression, and also
5 during social interactions with the opposite sex. It has been previously unclear how the brain
6 uses this complex multidimensional signal and generates a discrete action: the attack. Here we
7 find that the largest posterior target of the VMHvl, the lateral periaqueductal gray (IPAG)
8 encodes a simplified attack-selective signal during aggression. Single units in the IPAG exhibit
9 greater selectivity for the attack action during aggression than VMHvl neurons and a
10 subpopulation of neurons in the PAG exhibit short-latency, time-locked spiking relative to the
11 activity of jaw muscles for biting during attack. In addition, channelrhodopsin assisted circuit
12 mapping reveals a preferential projection from VMHvl glutamatergic cells to IPAG glutamatergic
13 cells. Using projection-specific fiber photometry, we find that this excitatory projection conveys
14 male-biased signals from the VMHvl to downstream glutamatergic PAG neurons that integrate
15 ongoing male-related activity over several seconds, which suggests that action-selectivity is
16 generated by a combination of both pre and postsynaptic filtering mechanisms.

17

18 **Keywords:** Aggression, circuit, hypothalamus, periaqueductal gray, social behavior, jaw
19 muscle

20

21 The VMHvl has emerged as a clearing house for socially relevant information,
22 responding during attack, but also exhibiting increased activity during sensory investigation of
23 males and females and during the preparatory phase prior to attack(Falkner et al. 2016, 2014;
24 Remedios et al. 2017; Lin et al. 2011). In addition, suppression of VMHvl activity decreases not
25 only the frequency of attack, but also investigatory, sexual, and aggression-seeking
26 behaviors(Yang et al. 2013; Lee et al. 2014; Falkner et al. 2016). How then do neurons

27 downstream of the VMHvl interpret this complex code to drive aggression? Pharmacological
28 manipulation of PAG circuits have been shown affect the efficacy of hypothalamic-mediated
29 conspecific aggression, strongly indicating that the PAG's actions are downstream of the
30 hypothalamus (Zalcman and Siegel 2006; Gregg and Siegel 2003), though its precise role in
31 this transformation has remained unclear. The emerging role of the PAG in the expression of
32 other innate behaviors, such as stimulus-induced flight, appears to be that of a split-second
33 action (Evans et al. 2018; Wang et al. 2019). We reasoned that a parallel circuit in the PAG
34 might perform a similar function during conspecific attack.

35 We reversibly suppressed the activity of the PAG during freely moving interactions with
36 males and females using the GABA_A agonist muscimol and tested whether inactivation altered
37 conspecific social behaviors, including attack and investigation. We found that inactivation of
38 the PAG produced action-specific deficits: we observed a decrease in time spent attacking a
39 male intruder, but no effect in the time spent investigating either males or females (Fig 1A-B,
40 Supplementary Movie 1). We observed a similar action-selectivity in the effects of muscimol on
41 attack across alternative measures of behavior including mean duration of each behavior,
42 latency to the first behavioral episode, number of behavioral episodes, and the total time spent
43 engaging in each particular behavior (Supplementary Fig1). We did not observe a reduction of
44 overall velocity during non-aggressive behaviors, suggesting that the effects of muscimol were
45 not due to locomotor deficits (Supplementary Fig 1).

46 The specificity of this deficit during PAG inactivation indicates that the PAG's role within
47 the aggression circuit is uniquely action-selective relative to the more complex role of the
48 VMHvl. To confirm this, we recorded populations of single neurons in the IPAG during free
49 interactions with males and females and compared the response profiles to newly quantified
50 measures of previously recorded neurons from the VMHvl (Falkner et al. 2014; Lin et al.
51 2011). We focused on the IPAG given the high amount of aggression-induced immediate early
52 gene expression observed in our previous studies (Lin et al. 2011). Electrode tracks in all

53 animals were confirmed to be located in the IPAG post hoc using Dil (Fig 1C). We recorded
54 from populations of neurons during freely moving interactions with males (10 minutes) and
55 females (10 minutes) and examined the firing rates of single units aligned to attack,
56 investigation of males, and investigation of females (Fig 1D-G). Across the population (n=164
57 neurons, 6 animals), we observed that a subpopulation of neurons in the IPAG exhibited their
58 peak firing aligned to the onset of attack while few neurons exhibited peak firing aligned to the
59 onset of either investigation of male or female conspecifics (Fig 1E-G).

60 This selectivity for attack differs substantially from the response properties of the VMHvl.
61 To directly compare these populations, we calculated the activity of each single unit in the
62 VMHvl and IPAG to attack, investigate male, and investigate female. We observed that across
63 the population, the VMHvl exhibits distinct activity peaks aligned to attack, investigation of
64 males, and investigation of females (Fig 1H, top). In contrast, the population response at the
65 PAG reveals an increase only during attack (Fig 1H, bottom). To compare the responses of
66 single neurons in these populations, each neuron was assigned a responsivity score for each
67 behavior (relative to its response during nonsocial behaviors). In addition, we determined the
68 number of Bonferroni-corrected, significant neurons for each behavior in both VMHvl and IPAG
69 populations (Fig 1I-J). We found that the population of IPAG neurons is significantly more
70 attack-selective than investigate-selective, while the VMHvl population has equal responsive
71 selectivity for both behaviors (Fig 1I). In addition, we found that IPAG exhibited an increased
72 number of uniquely attack responsive neurons, and showed a decrease of both co-selective and
73 investigate-selective single units relative to the VMHvl (Fig 1I, $p=0.0031$, chi-square test
74 comparing numbers of attack responsive and investigate-responsive neurons between VMHvl
75 and IPAG). Consistent with this, we also observed that the IPAG population shows little
76 selectivity for either male or female investigation, and, relative to the VMHvl, has fewer neurons
77 that respond to either or both of those behaviors (Fig 1J, $p=0.0210$, chi-square test comparing
78 numbers of investigate-male-responsive and investigate-female-responsive neurons between

79 VMHvl and IPAG). Overall, we found that the selectivity for attack (compared to other social
80 behaviors) was increased in the IPAG compared to the VMHvl and that the activity of attack
81 selective neurons in the VMHvl increased earlier than attack selective neurons in the IPAG (Fig
82 1K-L). Together these data are consistent with a role for the PAG in simplifying aggression-
83 relevant signals from the VMHvl to drive attack.

84 To further explore the action selectivity of the IPAG during aggression, we examined the
85 relationship between IPAG activity and an important effector for mouse aggression: the
86 jaw. Using intramuscular injections of a retrogradely transported pseudorabies virus (PRV)
87 (Smith et al. 2000), neurons in the PAG have been previously identified having polysynaptic
88 projections to jaw muscles critical for aggressive behavior (Fay and Norgren 1997). We injected
89 the superficial masseter muscle of the jaw (the critical muscle for jaw closure) with a GFP-
90 labeled PRV 152 and found that the majority of retrogradely labeled neurons were located in the
91 IPAG within the boundaries of the VMHvl excitatory terminal field (Supplementary Fig 2). We
92 next tested whether these jaw projecting neurons were activated during aggressive encounters
93 by examining the overlap between PRV-labeled GFP and the expression of an aggression-
94 induced immediate early gene, c-Fos. We found that there were many c-Fos expressing
95 neurons in the IPAG that were not GFP labeled, consistent with the idea that aggression may
96 recruit many effector-specific pools of neurons. However, we also found that GFP-labeled
97 neurons were far more likely than chance to also express attack-induced c-Fos (Fig. 2A-C),
98 indicating that these jaw-projecting neurons in the IPAG likely play a role in aggression.

99 We hypothesized that neurons in the IPAG may have a specific role in coordinating
100 attack-relevant musculature. Since the time course of immediate early gene expression is too
101 slow to resolve the temporal relationship between activity of PAG neurons and muscle activity,
102 we developed a preparation to simultaneously record from neurons in the IPAG and EMG
103 activity from the superficial masseter (EMG_{SM}) during interactions with males while animals are
104 attacking and performing other social interactions (Fig 2D-E, Supplementary Video 2, n=64

105 neurons in 4 animals). We used mutual information (MI) to quantify whether the EMG_{SM} signal
106 provides useful information in predicting the activity during male or female interactions. Mutual
107 information provides a model-free method for capturing the amount of joint information between
108 two signals, and increased mutual information indicates that one signal can be used to predict
109 the other (Srivastava et al. 2017). We calculated MI for each neuron and associated EMG_{SM}
110 signal relative to a circularly permuted time shuffled control during interactions with males and
111 females. We observed that across the population of recorded neurons, EMG_{SM} increased the
112 MI during male interactions but not during female sessions relative to shuffle control and also
113 that MI provided by the EMG_{SM} signal was significantly higher during male interactions compared
114 to female interactions (Fig 2F), indicating that a subpopulation of neurons is modulated during
115 attack-related jaw movement, but is not similarly activated by nonspecific jaw movements during
116 female interactions.

117 We hypothesized that the activity of jaw-activated neurons might have a tight temporal
118 relationship to the muscle activity if it is involved in directly activating the muscle. We examined
119 the relationship between individual spikes and the EMG_{SM} signal. For each neuron, we
120 generated a spike-triggered-EMG (STEMG) across an 800ms bin around each spike and used
121 strict criteria to determine whether each STEMG demonstrated a significant relationship with
122 individual spikes (Davidson et al. 2007). We found that a subpopulation of recorded neurons
123 (21.8%, 14/64 neurons) showed a significantly increased STEMG within 60 ms of spikes during
124 interactions with males ($\text{EMG}_{\text{sm+}}$, Fig 2G and I, black). Most but not all of these $\text{EMG}_{\text{sm+}}$
125 neurons (12/14) were activated during attack (Fig 2H and J, black). In addition, 9/64 neurons
126 were identified as being significantly activated during attack but showed no increase in STEMG
127 plot ($\text{EMG}_{\text{sm-}}/\text{Atk+}$, Fig 2I-J, red). Those $\text{EMG}_{\text{sm-}}/\text{Atk+}$ neurons often exhibited suppression
128 following PAG spiking (Fig 2I, red) and showed activation that persisted through the attack
129 responses (Fig 2J, red). These response patterns differ from those of the $\text{EMG}_{\text{sm+}}$ cells that
130 were increased only at the onset of attack (Fig. 2J, black). These data are consistent with the

131 hypothesis that attack-related neurons in the IPAG may activate multiple attack related muscles,
132 including jaw opening musculature. A smaller number of neurons (7.8%, 5/64 neurons)
133 exhibited a time-locked relationship during female interactions, suggesting that some jaw
134 responsive neurons may be recruited during other (nonaggressive) behaviors.

135 Though we did not explicitly test the activity of IPAG neurons during other nonsocial
136 behaviors, we found that similar to the VMHvl, the population of recorded IPAG neurons
137 exhibited decreased activity during spontaneous bouts of grooming and eating, indicating that
138 non-aggressive jaw relevant actions do not similarly activate IPAG neurons (Supplementary
139 Figure 3).

140 Our data demonstrates that neurons in the IPAG exhibit a greater degree of selectivity
141 for aggressive action (i.e. attack) than neurons in the VMHvl. One simple mechanism by which
142 this circuit could perform the transformation is if the projection from the VMHvl to PAG were a
143 labeled line for aggression-specific information. To test this directly, first we explored whether
144 excitatory projection neurons from the VMHvl form functional connections with neurons in the
145 IPAG. We targeted excitatory projection neurons by injecting a red-shifted cre-dependent
146 excitatory opsin (AAV2.Syn.Flex.ChrimsonR.tdTomato) into the VMHvl of vGlut2-ires-cre mice
147 crossed with an Ai6 reporter. This strategy allowed us to record postsynaptic responses from
148 vGlut2+ and vGlut2- neurons in the IPAG while optically manipulating the glutamatergic VMHvl-
149 PAG projection (Fig. 3A-B). We first confirmed that brief light pulses at the VMHvl were
150 sufficient to reliably evoke action potentials (Fig. 3C). Then, we made coronal slices of the IPAG
151 and performed voltage clamp recording from putative vGlut2+ and vGlut2- neurons (identified by
152 the presence and absence of GFP label) and tested whether a brief red light pulse activating the
153 VMHvl-PAG terminals was sufficient to evoke postsynaptic responses (Fig. 3D-E). We found
154 that approximately 50% (12/25) of identified vGlut2+ neurons exhibited short-latency excitatory
155 post-synaptic currents (EPSCs) upon light delivery, while no single vGlut2- neurons (n =9)
156 exhibited this excitatory response (Fig. 3F-G). Bath application of tetrodotoxin (TTX) and 4-

157 aminopyridine (4-AP) did not change the magnitude of light-evoked EPSCs, supporting the
158 monosynaptic nature of the connection (Fig. 3H-I). None of the recorded cells showed inhibitory
159 postsynaptic currents (IPSCs) upon light delivery.

160 Next, to explicitly test what information is being conveyed by this excitatory hypothalamic
161 to midbrain projection, we targeted excitatory VMHvl-PAG projecting neurons, by injecting the
162 ipsilateral side of a vglut2-ires-cre male mice with a retrogradely transported, cre-dependent,
163 calcium indicator (HSV-Ef1a-LS1L-GCaMP6f) into the IPAG. On the contralateral side of the
164 brain to the injection site, we also injected a cre-dependent calcium indicator
165 (AAV1.CAG.Flex.GCaMP6f.WPRE.SV40) in the VMHvl in order to compare the activity from the
166 total VMHvl vGlut2+ population, not specified by projection. We positioned fibers over both the
167 ipsi and contralateral VMHvl and used fiber photometry to simultaneously record respectively
168 from the VMHvl-PAG projection vGlut2+ neurons and the VMHvl general vGlut2+ population
169 during interactions with males and females (Fig 3J-K). We alternated between brief
170 presentations of a male mouse stimulus (~1 min) with a female mouse stimulus (~1 min) with a
171 1 min break between presentations (Fig 3L) and compared the normalized activity between the
172 VMHvl-PAG and VMHvl neuron populations across the entire set of interactions.

173 We found that both vGlut2+ VMHvl and VMHvl-PAG populations showed a strong bias
174 towards male compared to female mean activity (Fig 3M-N). However, in a direct comparison of
175 activity levels between VMHvl and VMHvl-PAG populations, we found that activity during male
176 interaction was not significantly different between these simultaneously recorded populations
177 (Fig 3O-P), while during female interactions, VMHvl-PAG activation decreased relative to the
178 overall VMHvl population response. In addition, to track how well the two signals match, we
179 computed the correlation (Pearson r) between the simultaneously recorded population activity of
180 VMHvl-PAG and VMHvl neurons and found that correlation coefficients during male interactions
181 were significantly increased during male interactions relative to female interactions across

182 animals (Fig 3Q), indicating that the VMHvl-IPAG projection conveys a more faithful copy of
183 population activity during male interactions than female interactions.

184 While we found that the VMHvl-PAG projection conveys male-biased information, we did
185 not observe that this pathway conveys action-selective information during aggression
186 (Supplementary Fig 4). To quantify this, we compared the PETHs of activity in the VMHvl
187 vGlut2+ population and the VMHvl-PAG vGlut2+ projection during attack and investigation of
188 males. We found that, similar to the single unit recording data, both VMHvl and VMHvl-PAG
189 neurons also showed clear activation peaks aligned to both attack and investigation of males
190 that were very strongly correlated at the level of the individual behavior episode (Supplementary
191 Fig 4A-C).

192 Together these data demonstrate that an excitatory projection from the VMHvl to the
193 IPAG conveys male-biased information to excitatory downstream populations, behaving as a
194 labeled line for aggression-relevant information. While this labeled line projection effectively
195 filters female-evoked signals, it does not filter non-attack signals during male interactions such
196 as investigation. This suggests that further mechanisms are needed to transform VMHvl activity
197 to an aggression-specific signal. One possibility is that the PAG is sensitive to slow temporal
198 features in its inputs prior to activation during attack, including investigation-evoked increases
199 that precede attack. To specifically model the interactions between the VMHvl and the PAG, we
200 performed simultaneous recordings of glutamatergic population (vGlut2+) in both areas during
201 free interactions with males and females (Fig. 3R-T). Qualitatively, we observed that during
202 male interactions, PAG activity peaks often followed VMHvl activity peaks, while during female
203 interactions, signal dynamics were more independent (Fig 3R-T, Supplementary Fig 4D-F). To
204 quantify these interactions, we computed the cross correlation of the simultaneously recorded
205 signals separately for male interactions, female interactions, and a baseline no-interaction
206 epoch. We found that the cross correlation during male interactions was strongly and
207 asymmetrically skewed across a multi-second timescale, indicating that increases in VMHvl

208 signals “lead” PAG signals during interactions with males, but not females (Fig. 3U-V). The
209 integral of the cross correlation during the “pre” epoch (VMHvl leads PAG) relative to the “post”
210 epoch (PAG leads VMHvl) significantly increased during male interactions across the population
211 of recorded animals (n=7, p=0.0174, paired t-test) and not significantly different during either the
212 interactions with females or no-interaction baseline period (p=0.9333, p=0.6148, paired t-test).

213 The slow temporal dynamics of the cross correlation during male interactions suggests
214 that PAG activity is influenced by VMHvl activity stretching backwards in time for several
215 seconds. To specifically quantify this temporal relationship between the VMHvl and IPAG, we
216 modeled the ongoing PAG activity using a time-varying linear regressive model. We iteratively
217 fit PAG activity with the activity of the VMHvl (VMHvl → IPAG) with a family of models with a
218 variable number of regressors representing increasing numbers of previous time bins, used
219 Akaike Information Criteria (AIC) to select the best model within each family, and cross
220 validated this model on a separate data set for each recorded animal. We performed this model
221 selection separately for male and female interactions and across a variety of bin sizes, ranging
222 from 50 ms to 1 s. We found that cross validated fits for the best fit model were significantly
223 better during male but not for female interactions relative to a time shuffled control. Importantly,
224 this effect was consistent across a range of bin sizes (Fig. 3W), indicating that this variable
225 made little difference in the model fit. In addition, we extracted the model order (number of time
226 bins) for the best fit model for each animal for male and female interactions for each bin size.
227 We found that the elapsed time associated with these best fit models was significantly longer for
228 male interactions than female interactions (Fig. 3W, right), indicating that during male
229 interactions, PAG signals are influenced by VMHvl signals stretching farther back in time.

230 On a conceptual level, this suggests that activity in the VMHvl increases for several
231 seconds prior to activation of the PAG, an effect consistent the action specificity of the PAG. As
232 a control, we also fit the reverse circuit model, (IPAG→ VMHvl) and found that both the fits, and
233 model order are significantly decreased relative with the forward circuit model during male, but

234 not female interactions (Supplementary Figure 5). Together, these results suggest a model by
235 which during interactions with males, but not during interactions with females, the PAG receives
236 VMHvl inputs conveying information about the sensory properties of the stimulus obtained
237 during investigation, and this information is integrated over many seconds in order to drive
238 attack behavior (Fig. 3X).

239 These findings provide evidence that the role of the PAG in the aggression circuit is to
240 transform the complex sensory-motor and motivational signals of the hypothalamus into
241 aggressive action and to coordinate the activation of effector-specific musculature, including the
242 jaw. These results add to a growing literature that position the PAG as a critical initiator of innate
243 behaviors that are determined by combinations of noisy sensory and state-dependent inputs
244 (Koutsikou, Apps, and Lumb 2017). Since PAG neurons are active later and more acutely
245 during attack behavior than its hypothalamic inputs from the VMHvl, it may serve as a
246 behavioral initiation threshold, as has been suggested for other innate behaviors. We do not
247 mean to suggest that the IPAG is “for” aggression: the PAG (and in particular hypothalamic to
248 PAG pathways) have been implicated in many innate sensory-driven behaviors including but not
249 limited to threat responsivity (Wang, Chen, and Lin 2015; Evans et al. 2018), prey capture(Li et
250 al. 2018), itch(Gao et al. 2018), oro-motor coordination(Stanek et al. 2014), and social
251 avoidance following defeat(Franklin et al. 2017). Additionally, the PAG has a well-documented
252 role across species in the generation of vocalization, a behavior that also requires the
253 integrations of social-sensory signals and the coordination of facial and laryngeal musculature
254 (Kittelberger, Land, and Bass 2006; Holstege 2014). Here we add to this growing literature by
255 elucidating the neural coding during conspecific attack and further hypothesize that the PAG is
256 capable of orchestrating many complex innate behaviors by coordinating output to relevant
257 muscles through sex-selective processing of slow temporal features in its inputs.

258

259

260 **Methods**

261

262 **Animals**

263 Experimental mice were sexually experienced, wild-type male C57BL/6N (12–24 weeks,
264 Charles River), wild-type male Swiss Webster (12–24 weeks, Taconic), *vGlut2*-ires-Cre mice.
265 Naïve *vGlut2* x *Ai6* mice were used for slice physiology and tracing experiments. Intruders were
266 either group housed, sexually inexperienced BALB/c males or C57BL/6 females (both 10–30
267 weeks). Mice were maintained on a reversed 12-h light/dark cycle (dark cycle starts at noon)
268 and given food and water *ad libitum*. All procedures were approved by the IACUC of NYULMC
269 in compliance with the NIH guidelines for the care and use of laboratory animals.

270

271 **Behavior analysis and tracking**

272 All freely moving behaviors were recorded using top and side GigE cameras using StreamPix
273 (Norpix) and all videos were manually annotated for pre-identified behaviors and tracked for
274 positional and velocity information using custom Matlab Software
275 (<https://github.com/pdollar/toolbox>). Behaviors were manually classified as previously described
276 (Falkner et al. 2014); individual behaviors included attack, investigation of males, investigation
277 of females, mounting, eating, and grooming. All interactions were “resident intruder assay” (5–
278 10 minutes of free interaction with male or female intruder), or alternating interactions with
279 males and females (1 min each) separated by 1 min (Fig 3).

280

281 **Pharmacological Inactivation**

282 For all pharmacological inactivations, double cannulae were implanted 0.5 mm above IPAG
283 (coordinates: -4.24mm,A-P, +/-0.5mm M-L, -1.85mm D-V) from and 0.2–0.3 μ l of either saline or
284 of 0.33 mg/ml muscimol (Sigma) in saline were injected into the PAG bilaterally through the

285 implanted double cannulae on alternating days. 8/11 animals were injected with fluorescent-
286 conjugated muscimol (0.5 mg/ml) prior to perfusion to confirm injection coordinates and injection
287 volume spread.

288

289 ***Extracellular recording of freely moving mice***

290 Methods for physiological recording in freely moving animals were described previously.
291 Custom-built 16-channel (or 14 channel with EMG) tungsten electrode bundles or groups of
292 tetrodes were attached to a moveable microdrive and implanted over the IPAG. After allowing 2
293 weeks for recovery, we connected the implanted electrode to a 16-channel headstage. Signals
294 were streamed into a commercial acquisition system through a torqueless, feedback-controlled
295 commutator (Tucker Davis Technology) and band-pass filtered between 100 and 5,000 Hz.
296 Digital infrared videos of animal behavior from both side- and top-view cameras were
297 simultaneously recorded at 640×480 pixel resolution at 25 frames per second (Streampix,
298 Norpix). Video frame acquisition was triggered by a TTL pulse from the acquisition system to
299 achieve synchronization between the video and the electrophysiological recording. Spikes were
300 sorted manually using commercial software (OfflineSorter, Plexon) based on principal
301 component analysis. Unit isolation was verified using autocorrelation histograms. To consider
302 the recorded cell as a single unit, cells had to have a signal/noise ratio >2; spike shape had to
303 be stable throughout the recording; and the percentage of spikes occurring with inter-spike
304 intervals (ISIs) <3 ms (the typical refractory period for a neuron) in a continuous recording
305 sequence had to be <0.1%. We checked for redundancies within days by examining the cross
306 correlations of co-recorded neurons and checked for redundancies across days by comparing
307 waveforms and temporal response profiles. After the first recording, the implanted electrode
308 was slowly moved down in 40-μm increments. The placement of the electrode was examined
309 histologically with the aid of Dil coated on the electrodes. Animals were excluded if electrodes

310 were not confined to the PAG. Recordings of the VMHvl (Fig 1H-L) were performed previously
311 using identical methods (Falkner et al. 2014; Lin et al. 2011) and reanalyzed here for direct
312 comparison to PAG neurons.

313

314 ***Electrophysiology Analysis***

315 Spikes in single neurons were convolved with a 25 ms Gaussian for presentation (Fig
316 1D). Responsivity index for each behavior (Fig 1i-j) was computed as

317 $(\text{Activity}_{\text{behavior}} - \text{Activity}_{\text{baseline-nonsocial}}) / (\text{Activity}_{\text{behavior}} + \text{Activity}_{\text{baseline-nonsocial}})$

318 Where $\text{Activity}_{\text{behavior}}$ is defined as the mean activity across all episodes of a particular behavior
319 (e.g. attack) and $\text{Activity}_{\text{baseline-nonsocial}}$ is defined as the mean activity across all episodes designated
320 as non-social within the given social interaction. Within-neuron significance was determined
321 using a paired t-test for each neuron (behavior vs. nonsocial) compared to a Bonferroni-
322 corrected threshold for each tested population.

323

324 ***PRV injections***

325 The right masseter was exposed and PRV-152 (kind gift from Lynne Enquist), was injected at 5
326 separate locations, 250uL per injection along the A-P axis of the muscle. The skin was sutured
327 closed and PRV was incubated for 96-112 hrs prior to sacrifice. In some cases, animals were
328 allowed to freely interact with a male mouse for 10 min 1 hour prior to sacrifice at the 96 hr time
329 point post-PRV injection. These animals were stained for c-Fos (primary antibody: goat anti-
330 Fos, Santa Cruz, sc-52G, 1:300, secondary antibody: donkey anti-goat Dylight 549, Jackson
331 Immuno, 705-505-147, 1:300).

332

333 ***EMG implantation and recording***

334 To perform simultaneous recordings of PAG neurons and jaw muscle activity, we implanted
335 animals with chronic EMG electrodes in the right masseter superficial muscles of the
336 jaw. Electrodes were constructed using a pair of 0.001 inch flexible multi-strand stainless steel
337 wires (A-M Systems, No. 793200) with the insulation removed from a 0.5-mm segment of each
338 wire such that pairs of electrodes recorded signals from separate but nearby areas of the same
339 muscle. Electrode wires were threaded through the muscle during a surgical procedure and
340 anchored with a knot on the outside of the muscle. EMG wires were then threaded under the
341 skin to the base of the skull where they were attached to ground electrodes. EMG wire output
342 was relayed through a preamplifier and commutator to the digitizer with a sampling rate of 3,000
343 Hz (Tucker Davis Technology). Signals were processed by taking the difference from the pair of
344 electrodes, and this differential signal was low pass filtered at 300 Hz.

345

346 **EMG analysis**

347 *Mutual Information*

348 Mutual information was computed between simultaneously recorded PAG activity and jaw
349 EMG. EMG signals were rectified, low pass filtered at 20Hz, and downsampled to 1kHz. Spike
350 trains were converted into a continuous instantaneous firing rate (IFR) with the same number of
351 points as the downsampled EMG signals. For each pair of recorded PAG instantaneous firing
352 rate and EMG signal, the continuous signals were discretized and MI was computed according
353 to the definition(Shannon and Weaver 1964; Schilling, n.d.; Timme and Lapish 2018):

$$354 MI(X;Y) = \sum_{x,y} P_{XY}(x,y) \log P_{XY}(x,y) P_X(x) P_Y(y) = E_{P_{XY}} \log P_{XY} P_X P_Y$$

355 Where x and y represent the instantaneous firing rate and EMG signal respectively.

356 For each signal pair, the MI was compared relative to the mean of ten iterations of a
357 circularly permuted time shuffled control.

358 *Spike Triggered EMG*

359 STEMGs were computed on rectified EMG signals by averaging the EMG signal in an 800ms
360 window around each PAG spike recorded during interactions with a male or with a
361 female. STEMGs were computed separately for each 10s increment during male and female
362 interactions, smoothed with a 5ms moving average, then normalized by the number of spikes.
363 To correct for drift due to volleys of successive spikes, STEMGs were baseline corrected by
364 subtracting a baseline 100ms boxcar filtered version of the STEMG. To determine whether
365 STEMGs contained significant peaks, we set strict criteria: STEMGs had to have a minimum of
366 5 consecutive points that crossed above the 98% confidence interval within 60ms of the 0 (the
367 spike onset).

368

369 ***In vitro* electrophysiological recordings**

370 Vglut2:Cre x Ai6 mice were injected with 100 nL rAAV2.syn.flex.ChrimsonR.tdT into VMHvl. Three
371 weeks after virus injection, acute horizontal brain slices of VMHvl and PAG (275 μ m in thickness)
372 were collected using standard methods (Fang et al. 2018). After being anesthetized by isoflurane
373 inhalation, the mice were perfused by ice-cold choline based cutting solution containing (in mM)
374 25 NaHCO₃, 25 glucose, 1.25 NaH₂PO₄, 7 MgCl₂, 2.5 KCl, 0.5 CaCl₂, 110 choline chloride, 11.6
375 ascorbic acid, and 3.1 pyruvic acid. The slices were collected in the same cutting solution using
376 a Leica VT1200s vibratome, incubated for 20 min in oxygenated artificial cerebrospinal fluid
377 (ACSF) solution (in mM: 125 NaCl, 2.5 KCl, 1.25 NaH₂PO₄, 25 NaHCO₃, 1 MgCl₂, 2 CaCl₂ and
378 11 glucose) (osmolality, 295 mmol/kg) at 32–34°C and then maintained at room temperature until
379 use. Standard whole cell recordings were performed with MultiClamp 700B amplifier (Molecular
380 Devices) and Clampex 11.0 software (Axon Instruments). Membrane currents were low-pass

381 filtered at 2 kHz and digitized at 10 kHz with Digidata 1550B (Axon Instruments). Electrode
382 resistances were 2–4 MΩ, and most neurons had series resistance from 4 to 15 MΩ.
383 Glutamatergic (green fluorescent) or GABAergic (non-fluorescent) cells as well as Chrimson-
384 tdTomato expressed VMHvl cells were identified with an Olympus 40 x water-immersion objective
385 with GFP and TXRED filters. The slices were superfused with ACSF warmed to 32– 34°C and
386 bubbled with 95% O₂ and 5% CO₂. The intracellular solutions for voltage clamp recording
387 contained (in mM) 135 CsMeSO₃, 10 HEPES, 1 EGTA, 3.3 QX-314 (Cl⁻ salt), 4 Mg-ATP, 0.3 Na-
388 GTP, and 8 Na₂-Phosphocreatine (osmolality, 295 mmol/kg; pH 7.3 adjusted with CsOH), and for
389 current clamp recording contained (in mM) 130 K MeSO₃, 5 KCl, 0.5 EGTA, 20 HEPES, 1.8 MgCl₂,
390 0.1 CaCl₂, 4 Na₂-ATP, and 0.2 Na-GTP (osmolality, 295 mmol/kg; pH 7.3 adjusted with KOH). To
391 activate Chrimson-expressing VMHvl glutamatergic neurons and Chrimson-expression axons in
392 PAG, brief pulses of full field illumination (20 ms for VMHvl during current clamp recording and 1
393 ms duration for PAG during voltage clamp recording) were delivered onto the recorded neuron
394 with 605 nm LED light (pE-300white; CoolLED) at 35 s intervals. Voltage clamp recording was
395 conducted for PAG neurons, and the membrane voltage was held at -70 mV for EPSC recording,
396 and at 0 mV for IPSC recording. Current clamp recording was conducted in VMHvl glutamatergic
397 neurons expressing Chrimson-tdTomato, where the neurons were maintained at resting potential
398 and spiking activity was detected with or without red light pulses (20 ms, 20 Hz for 500 ms).
399

400 ***Fiber photometry recordings***

401 A rig for performing simultaneous fiber photometry recordings from 2 locations was constructed
402 following basic specifications previously described with a few modifications. For simultaneous
403 VMH and VMHvl-PAG recordings, we injected vGlut2-ires-cre males with 100-160nl of
404 AAV1.CAG.Flex.GCaMP6f.WPRE.SV40 (Lot CS0956, CS0845, CS0224WL, Upenn, final titer::
405 9.3×10^{12} PFU/ml) ipsilaterally into the VMHvl, and 240nl of HSV-Ef1a-LS1L-GCaMP6f (MIT
406 vector core, Lot RN506, final titer: 1.0×10^9 PFU/ml) contralaterally in the PAG. For
407 simultaneous recordings of the VMHvl and IPAG, we injected 80-120nl of AAV2/1 CAG::Flex-
408 GCaMP6f-WPRE-SV40 ipsilaterally into the VMHvl, and 160-240nl of AAV2/1 CAG::Flex-
409 GCaMP6f-WPRE-SV40 in the IPAG. Viruses were injected using the following
410 coordinates: VMHvl (-1.82A/P, 0.72M/L, -5.8D/V), IPAG(-3.64A/P, 0.5M/L-2.4D/V).
411 A 400- μ m optic fiber (Thorlabs, BFH48-400) housed in a metal ferrule (Thorlabs, SFLC440-10)
412 was implanted 0.4 mm above each injection site, except for the HSV-Ef1a-LS1L-GCaMP6f
413 injection, where the fiber was placed over the VMHvl. After three weeks of viral incubation and
414 before recording, a matching optic fiber was connected to the each implanted fiber using a
415 ferrule sleeve. A 400-Hz sinusoidal blue LED light (30-50 μ W) (LED light: M470F1; LED driver:
416 LEDD1B; both from Thorlabs) was bandpass filtered (passing band: 472 ± 15 nm, Semrock,
417 FF02-472/30-25) and delivered to the brain to excite GCaMP6. The emission light then traveled
418 through the same optic fiber, was bandpass filtered (passing band: 534 ± 25 nm, Semrock,
419 FF01-535/50), detected by a femtowatt silicon photoreceiver (Newport, 2151) and recorded
420 using a real-time processor (RZ5, TDT). The envelope of the 400-Hz signals that reflects the
421 intensity of the GCaMP6 signals were extracted in real-time using a custom TDT program.
422 Baseline adjusted fluorescence signals were regressed using a 30s spline approximation.
423

424 **Histology and imaging**

425 Animals were deeply anaesthetized using 0.5 ml of a ketamine-xylazine cocktail (10 mg/ml
426 ketamine and 5 mg/ml xylazine) and transcardially perfused with phosphate buffered saline
427 (PBS) followed by cold 4% paraformaldehyde in PBS. Brains were immersed overnight in a 20%
428 sucrose solution, embedded with cutting medium (Tissue-Tek) and sectioned using a cryostat
429 (Leica). Standard immunohistochemistry procedures were followed to stain 30- μ m coronal brain
430 sections for all mice. DAPI (1:20,000, Life Technologies, catalog number D21490, widely
431 validated) was used to assess electrode track for physiology and fiber track for photometry. We
432 acquired 2.5 \times or 5 \times fluorescent images to determine cannula or electrode placements. We used
433 10 \times fluorescent images to count c-Fos+ and PRV+. Cell counting was done manually using
434 ImageJ on 30- μ m sections separated by 60 μ m that had observed GFP label in the IPAG.

435
436 **Time-varying linear regression model**

437 We modeled the population response of the PAG during male and female interactions for each
438 animal by fitting the PAG response during each interaction including 10s prior to the introduction
439 and 10s following the removal of the animals with a series of autoregressive models using time-
440 varying lengths of simultaneously recorded VMHvl signal as the variable regressors using the
441 form:

442
$$PAG(t) = a_1 * VMHvl(t) + a_2 * VMHvl(t-1) + a_3 * VMHvl(t-2) + \dots + a_n * VMHvl(t-n)$$

443 where t represents the current time bin and the other regressors represent variable amounts of
444 elapsed time. PAG and VMHvl signals were binned in either 50ms, 100ms, 250ms, 500ms, and
445 1s bins and models were fit independently for each of these bin sizes. For each VMHvl and
446 PAG signal, data was halved and the first half was used to fit and the second half was used to
447 cross validate, using least squares. Model order was set to maximum value of 10s of elapsed
448 time, set independently for each bin size. For each family of models fit to the data, the best
449 order model was determined using AIC (Akaike Information Criteria) on the fit to the cross
450 validated data. A timeshifted null model was fit by circularly permuting the input data (VMHvl)

451 signal and fitting the unpermuted PAG signal, and fit and model order were re-fit for the
452 timeshifted data. Model order for the selected model was converted to elapsed time for each
453 binsize. Fits were performed separately for male and female interactions. Additionally, we
454 tested the alternative hypothesis that PAG signals influence VMHvl signal by fitting the “reverse”
455 model of the form:

$$456 \quad \text{VMH}(t) = a_1 \text{PAG}(t) + a_2 \text{PAG}(t-1) + a_3 \text{PAG}(t-2) + \dots + a_n \text{PAG}(t-n)$$

457 A similar model family was fit for the reverse model, and the model order (and elapsed time)
458 was determined for each model independently for each bin size.

459
460 **Statistical Analysis**

461 Parametric tests, including Student’s *t*-test, paired *t*-test, and two-sample *t* test were used if
462 distributions passed Kolmogorov–Smirnov tests for normality. For within-neuron tests of firing
463 rate significance, a non-parametric Wilcoxon signed rank test was used since spike rates were
464 often low and not normally distributed. Repeated tests of significance were corrected with a
465 strict Bonferroni correction. For all statistical tests, significance was measured against an alpha
466 value of 0.05 unless otherwise stated. All error bars show s.e.m. No statistical methods were
467 used to predetermine sample sizes, but our sample sizes are similar to those reported in
468 previous publications. Data collection and analysis were not performed blind to the conditions
469 of the experiments.

470 Statistical analyses used in each figure are listed below.

471 Figure 1. (B) Single factor, repeated measures ANOVA. (D) Single neuron activity average
472 using 25ms Gaussian smoothing (E-G) Top panels are the z-scored responses of individual
473 neurons aligned to each behavior, and histograms represent the number of neurons whose
474 peak response lies at that bin relative to behavior onset. Dotted line represents chance level
475 (number of bins/number of neurons). (I-J) Wilcoxon signed rank test for comparison of
476 population response. Percentages of neurons in pie charts computed using within-neuron

477 significance test across one or both behaviors, with Bonferroni correction. (K) Kolmogorov-
478 Smirnov test (L) Unpaired ttest across all bins using Bonferroni corrected threshold across all
479 bins.
480 Figure 2. (C) Paired t-test, (f) Kolmogorov-Smirnov test between cumulative distributions. (G)
481 Significant EMGsm+ neurons see methods.
482 Figure 3. (F) Fisher's test, (H) paired t-test, (M-Q) Error bars show +/-SEM, comparisons of
483 means with paired t-test. (U) Error bars show +/-SEM (V) Wilcoxon signed rank test of male,
484 female, and baseline activity. (W) Paired t-test between forward and null model at each bin for
485 fit, Paired t-test between male and female interactions for model time.
486 Supplementary Figure 1. (A-F) Paired t-test.
487 Supplementary Figure 2. (C) Paired t-test.
488 Supplementary Figure 3. (A-C) Wilcoxon signed rank test.
489 Supplementary Figure 4. (A-B,D-E) Activity shown is z-scored across the whole interaction
490 trace. (C,F) Activity for each individual behavior is baseline subtracted using a 1s bin 5s prior to
491 interaction. Individual behaviors compared using student's ttest, and comparison between
492 behaviors using an unpaired t-test.
493 Supplementary Figure 5. (A-B) Paired t-test between forward and reverse model at each bin.
494
495
496

497 **Figure Legends**

498

499 Figure 1. IPAG is more attack selective than the VMHvl. We recorded the behaviors during
500 freely moving social interactions with males and females during reversible inactivation (A-B) and
501 single unit recording (C-G). (B) Reversible inactivation of PAG using alternating injections of
502 saline and muscimol induced selective deficits on attack and no change in investigatory
503 behaviors (N = 11, *p=0.0134 for attack, left; p=0.985 for investigate male, middle; p=0.896 for
504 investigate female, one-way repeated measures ANOVA). (C) Histology showing example
505 placement of electrode bundle in the IPAG and electrode track locations for all recording
506 animals (N=6). (D) Example raster plot (top) and PETH (bottom) for activity of an example IPAG
507 units aligned to attack (red), investigation of a male (blue), and investigation of a female
508 (green). (E-G) Normalized responses of population (top) of recorded neurons sorted by peak of
509 response aligned to attack (E, N = 159), investigation of male (F, N = 158), and investigation of
510 female (G, N = 151). Bottom histograms show number of units with response peak above 95%
511 CI in each bin. Dotted black lines (E-G) represent chance levels for each behavior. (H)
512 Normalized population response mean \pm SEM of VMHvl (top) and IPAG (bottom) during onsets
513 of key behaviors interactions with males: attack (red) and investigate male (blue), and with
514 females: investigate female (green). (N = 166,156 for VMHvl male attack and investigate,
515 N=212 for female investigate, N = 159 for IPAG male attack and investigate, N=151 for female
516 investigate). Comparison of responsivity of individual VMHvl neurons (I-J top, light gray) and
517 IPAG neurons (I-J bottom, dark gray). VMHvl population is nonselective between attack and
518 investigate male (I, top, p=0.806, N = 157), and selective for investigation of male compared to
519 female (J, top,p=0.005, N=147), while IPAG is selective for attack relative to investigate male (I,
520 bottom, p=3.4x10⁻⁷, N=152), and nonselective for investigation of males and females (J,
521 bottom, p=0.415, N=152). Tests in I-J performed using Wilcoxon signed-rank test. Pie chart
522 insets displaying percentages of individually significant neurons (Bonferroni-corrected t-test) in

523 VMHvl and IPAG show an increasing number of purely attack selective neurons in the IPAG
524 relative to VMHvl and a decrease of investigation selective neurons in the IPAG. (K) Selectivity
525 of population to attack compared to selectivity to investigate male shows that attack-shifted
526 peak for IPAG population (dark gray) relative to VMHvl (light gray). $P=0.0001$, Kolmogorev
527 Smirnov test. (L) Attack responsive neurons in the VMHvl (light gray) have significantly
528 increased activity prior to attack onset relative to attack responsive IPAG neurons (dark
529 gray). $N= 44$ neurons in VMHvl $N=46$ neurons, IPAG, $p = 0.0005$, Bonferroni corrected
530 unpaired ttest across all bins.

531
532 Figure 2. IPAG spiking has precise temporal alignment with jaw muscle activity during
533 aggression. (A) Experimental design for injections of PRV-152 into the superficial masseter of
534 the jaw, followed by 10min aggressive interaction for c-Fos induction after 96 hrs of viral
535 incubation. (B) Example histology showing GFP labeling in the IPAG is co-localized with
536 aggression-induced c-Fos. Panels show insets (white box) of c-Fos (mCherry, left top), PRV-
537 GFP (left center), and merge (left bottom) with arrows indicating neurons with overlap. (C)
538 PRV-GFP labeled cells show preferential overlap with aggression-induced c-Fos ($p = 0.009$, $N =$
539 3, paired t-test). (D) Example simultaneous recordings of jaw EMG and IPAG spiking during
540 attack episodes. (E) Example EMG (top) and activity from simultaneously IPAG neuron
541 (bottom) during interaction with a male (F) Mutual information (MI) of IPAG spiking and EMG
542 activity comparing during interactions with males and females ($N=64$ neurons). MI of activity
543 during male interaction compared to time shuffled control ($p=0.0214$, paired t-test), MI of activity during
544 female interactions to time shuffled control ($p=0.1551$, paired t-test), MI of activity during
545 male and female interactions ($p=0.0053$, paired t-test). Example STEMG (G) and attack-aligned
546 PETH (H) with precise temporal alignment to EMG. (I-J) STEMG (I) and attack aligned activity
547 (J) of neurons with significant STEMG (red, top trace), and significant attack responsive neurons
548 that are do not have significant STEMG (black, bottom trace), show distinct dynamics.

549
550 Figure 3. An excitatory VMHvl-IPAG projection filters aggression-relevant information using pre
551 and post-synaptic mechanisms. (A) Viral strategy for targeting excitatory projections from
552 VMHvl to IPAG using vGlut2-ires-cre x Ai6 mice. Slices were made of VMHvl and IPAG and
553 whole cell recordings were performed. (B) Representative infrared differential interface contrast
554 image (IR-DIC) from a recorded slice containing VMHvl (top, left) and IPAG (bottom, left).
555 Yellow arrows indicate locations of recording pipette tips. Scale bar 500 μ m. (right) Coronal
556 section (right) showing expression of Chrimson-tdTomato (red) from a vGlut2 x Ai6 mouse.
557 Scale bar 1mm. (C) Example trace showing current clamp recording of a VMHvl glutamatergic
558 neuron expressing Chrimson-tdTomato. 605 nm light pulses (20 Hz, 20 ms for 500 ms, red
559 ticks) reliably evoked time-locked spiking. Scale bars: 100 ms (horizontal) and 10 mV (vertical).
560 (D) Histological image showing distribution of glutamatergic cells (green) and Chrimson-
561 tdTomato expressing fibers from the VMHvl (red) in the PAG. Blue: Topro-3. Scale bar, 200 μ m.
562 (E) Enlarged views from (D) showing biocytin-filled vGlut2 negative (top row) and positive cells
563 (bottom row) and their corresponding recording traces showing 1ms 605 nm light evoked EPSC
564 (-70 mV) and IPSC (0 mV). Yellow arrows indicate the locations of the biocytin filled cells. Scale
565 bar (left), 20 μ m. Scale bars (right): 100 ms (horizontal) and 10 pA (vertical). (F) Stacked bar
566 graphs showing the percentage of recorded PAG cells receiving EPSC during light stimulation.
567 12 out of 25 PAG vGlut2+ neurons received glutamatergic input from VMHvl, none showed light
568 evoked IPSC; none of 9 vGlut2- neurons showed any light evoked responses. Fisher's test. *p <
569 0.05. (G) Light-evoked EPSC amplitude (left) and latency (right) in PAG glutamatergic neurons
570 (n=12). Error bars show means \pm SEM. (H) Example traces showing 1ms 605 nm light evoked
571 EPSC before (black) and after 1 μ M TTX and 100 μ M 4AP perfusion (red) in PAG glutamatergic
572 neurons. Scale bars: 100 ms (horizontal) and 10 pA (vertical). (I) No change in light-evoked
573 EPSC amplitude before and after 1 μ M TTX and 100 μ M 4AP perfusion in PAG glutamatergic
574 neurons (n=6). Paired t-test. p > 0.05. (J) Experimental configuration of bilateral injection of

575 Cre-dependent GCaMP6f into Vglut2-ires-Cre mice for simultaneous fiber photometry
576 recordings of VMHvl and VMHvl-PAG projection neurons. Ipsilateral injection targets vGlut2+
577 VMHvl neurons and the contralateral injection targets vGlut2+ VMHvl-PAG projection neurons.
578 (K) Example histology of GCaMP-labeled vGlut2+ VMHvl neurons (right) and Vglut2+ VMHvl-
579 IPAG neurons (left) and placement of fiber tracks. (L) Example simultaneous recording of
580 vGlut2+ VMHvl (black) and VMHvl-PAG (magenta) projection neurons during alternating
581 interactions with males (blue) and females (red). (M-N) Population activity (mean +SEM for
582 each animal, N=6 animals) of comparison between activity during male interaction and female
583 interaction for VMHvl neurons (M, p=0.0062) and for VMHvl-PAG projection neurons (N,
584 p=0.0002), shows that both populations exhibit increased activity to males. (O-P) Comparison of
585 simultaneously recorded activity VMHvl and VMHvl-PAG neurons is not significantly different
586 during male interactions (O, p=0.3676), but activity during female interaction is reduced in
587 VMHvl-PAG neurons (P, p=0.044). (Q) Correlation of simultaneously recorded VMHvl and
588 VMHvl-PAG neurons is higher in male interactions than female interactions (p=0.0238). All
589 tests (M-Q) using paired t-test. (R) Experimental configuration of simultaneous recording of
590 vGlut2+ populations in the VMHvl and IPAG. VMHvl and IPAG were recorded during
591 interactions with males (S) and females (T). (U) Cross correlation of simultaneously recorded
592 signals during male interactions (blue), female interactions (red) and no-interaction baseline
593 (black). (V) Comparison of summed cross correlation in pre epoch (-10s to 0s) and post epoch
594 (0s to 10s) for male, female, and no-interaction baseline shows significant asymmetry only
595 during male interaction (N=7 animals, male p=0.0174*, female p=0.9333, baseline
596 p=0.6148). (W) PAG activity was fit with a linear model using a variable amount of preceding
597 VMHvl signal as the regressors. Fit percent (middle) and time (right) associated with best fit
598 models of cross-validated data using a time-varying input from VMHvl. Dotted lines represent
599 data from time shuffled controls. (X) Conceptual model of pathway selectivity of male-
600 responsive information.

601

602 Supplementary Figure 1.

603 Alternative measures of behavior, including behavior duration, latency to first behavior, number
604 of behavior episodes, and total time spent engaging the behavior confirm reduction of
605 aggression. Behaviors shown are attack (A, **p=0.00284, *p=0.0121, **p=0.0090, **p=.00689),
606 investigation of male (B, p=0.7344, p=0.8617, p=0.8091, p=0.8719), investigation of females (C,
607 p=0.6784, p=0.4077, p=0.2029, p=0.1322), and mounting behavior (D, p=0.1490, **p=0.0036,
608 p=0.3830, p=0.2329). Mean saline shown in light bars, muscimol shown in dark bars.
609 Reversible inactivation during male interaction reduces mean resident velocity (E), but effects
610 are eliminated when episodes of attack are removed from analysis (E, right inset). Inactivation
611 during female interaction has no effect on resident velocity (F). (N=11 animals for all
612 comparisons, *p<0.05, **p<0.01, ***p<0.001, ns=nonsignificant, paired ttest).

613
614 Supplementary Figure 2. PRV-labeled jaw-projecting neurons are maximally within VMHvl-
615 projection-defined column boundaries. (A) Experimental procedure for determining overlap
616 between VMHvl projection fields and PRV label. (B) Example histology showing VMHvl
617 synaptophysin-containing terminals (left), PRV-GFP labeled jaw-projecting neurons (center),
618 and overlap (right). (C) Number of GFP labeled neuron observed within each PAG column. N=4
619 animals, p=0.0028, one-way ANOVA (D) Putative circuit from excitatory vGlut2+ neurons to jaw.

620
621 Supplementary Figure 3. Other jaw-related behaviors decrease IPAG activity. (A-B) Activity
622 during eating is significantly decreased relative to attack (A, N=26, p=0.0007), and nonsocial
623 epochs (B, N=26, p=0.0006). Gray dots represent single neurons tested in both behaviors. (C)
624 Activity during grooming is decreased relative to nonsocial epochs (N=87, p=0.004). (D)
625 Neurons with significant STEMG activity do not show activity increases aligned eating or

626 grooming onsets, but do show activity aligned to attack. All pairwise comparisons done with
627 Wilcoxon signed rank test.

628
629 Supplementary Figure 4. Fiber photometry responses to individual male behaviors during
630 simultaneous recordings. (A-B) PETHs comparing simultaneously recorded mean VMHvl
631 (black) and VMHvl-IPAG (magenta) aligned to attack (A) and investigate male (B) N=6
632 animals. (C) Comparison of individual behavior episodes for attack (red) and investigate male
633 (blue). Both attack and investigate male acutely increase VMHvl and VMHvl-IPAG responses
634 (**p=9.2157*10^-13, ***p=1.3144*10^-6, N=84 attack episodes in 6 animals; ***p=1.8445*10^-
635 7, ***p=2.6243*10^-7, N=85 investigate male episodes in 6 animals, one sample
636 ttest; Comparison between behaviors, VMHvl: ***p=5.157*10^-4, VMHvl-IPAG: p=0.4201). (D-
637 E) PETHs comparing simultaneously recorded mean VMHvl (black) and IPAG (magenta)
638 aligned to attack (D) and investigate male (E) N=7 animals. (F) Comparison of individual
639 behavior episodes for attack (red) and investigate male (blue). Attack acutely increases VMHvl
640 and IPAG (**p=2.9198*10^-11, ***p=4.0921*10^-5, N=84 attack episodes in 6 animals), but
641 investigate only increases VMHvl (**p=2.1263*10^-5, p=0.5164, N=85 investigate male
642 episodes in 7 animals, one sample ttest). Comparison between behaviors, VMHvl:
643 ***p=5.157*10^-4, VMHvl-IPAG: p=0.4201). IPAG responses are significantly different between
644 attack and investigate, while VMHvl responses are not (VMHvl: p=0.1467, IPAG:
645 ***p=5.7677*10^-4, N=84 attack episodes, N=85 investigate male episodes in N=7 animals,
646 unpaired ttest).

647
648 Supplementary Figure 5. Comparison of forward (VMHvl → IPAG) and reverse (IPAG →
649 VMHvl) regressive models. Model fit percentages and model time for fits during male (A) and
650 female (B) interactions. Black traces (A-B) show reverse models. During male interactions
651 (blue), fits are significantly increased in forward model relative to reverse model (*p<0.05, paired
652 t-test for each time bin).

653

654 Supplementary Movie 1. Pharmacological inactivation of the PAG using muscimol results in
655 aggression-specific deficits. Example intermale aggression following saline infusion, compared
656 with behavior following muscimol inactivation. During inactivation, intermale aggression is
657 decreased while investigatory behaviors and other social behaviors are unchanged.

658

659 Supplementary Movie 2. Example of single IPAG neuron recorded simultaneously with EMG in
660 the superficial masseter muscle of the jaw with corresponding behavior. IPAG neuron (bottom
661 trace) shows time-locked spiking with EMG peaks (top trace).

662

663 **Author contributions**

664 ALF designed and carried out *in vivo* physiology and photometry experiments, performed all
665 analysis and modeling for these experiments, and wrote the manuscript. DW conducted slice
666 physiology experiments, analyzed the data and co-wrote the manuscript. AS assisted with PRV
667 tracing experiments, LWW and IZC performed pharmacological inactivation experiments. JEF
668 constructed microdrives associated with *in vivo* physiology experiments. DL conceived the
669 project, suggested experiments, analyzed data and edited the manuscript.

670

671 **Declaration of interest**

672 The authors declare no competing interests.

673

674

675 **References**

676 Davidson, A.G., O'Dell, R., Chan, V., and Schieber, M.H. (2007). Comparing effects in spike-
677 triggered averages of rectified EMG across different behaviors. *J. Neurosci. Methods* 163, 283–
678 294.

679 Evans, D.A., Stempel, A.V., Vale, R., Ruehle, S., Lefler, Y., and Branco, T. (2018). A synaptic
680 threshold mechanism for computing escape decisions. *Nature* 558, 590–594.

681 Falkner, A.L., Dollar, P., Perona, P., Anderson, D.J., and Lin, D. (2014). Decoding ventromedial
682 hypothalamic neural activity during male mouse aggression. *J. Neurosci.* 34, 5971–5984.

683 Falkner, A.L., Gosenick, L., Davidson, T.J., Deisseroth, K., and Lin, D. (2016). Hypothalamic
684 control of male aggression-seeking behavior. *Nat. Neurosci.* **19**, 596–604.

685 Fang, Y.-Y., Yamaguchi, T., Song, S.C., Tritsch, N.X., and Lin, D. (2018). A Hypothalamic
686 Midbrain Pathway Essential for Driving Maternal Behaviors. *Neuron* **98**, 192–207.e10.

687 Fay, R.A., and Norgren, R. (1997). Identification of rat brainstem multisynaptic connections to
688 the oral motor nuclei using pseudorabies virus. I. Masticatory muscle motor systems. *Brain Res.*
689 *Brain Res. Rev.* **25**, 255–275.

690 Franklin, T.B., Silva, B.A., Perova, Z., Marrone, L., Masferrer, M.E., Zhan, Y., Kaplan, A.,
691 Greetham, L., Verrechia, V., Halman, A., et al. (2017). Prefrontal cortical control of a brainstem
692 social behavior circuit. *Nat. Neurosci.* **20**, 260–270.

693 Gao, Z.-R., Chen, W.-Z., Liu, M.-Z., Chen, X.-J., Wan, L., Zhang, X.-Y., Yuan, L., Lin, J.-K.,
694 Wang, M., Zhou, L., et al. (2018). Tac1-Expressing Neurons in the Periaqueductal Gray
695 Facilitate the Itch-Scratching Cycle via Descending Regulation. *Neuron*.

696 Gregg, T.R., and Siegel, A. (2003). Differential effects of NK1 receptors in the midbrain
697 periaqueductal gray upon defensive rage and predatory attack in the cat. *Brain Res.* **994**, 55–
698 66.

699 Holstege, G. (2014). The periaqueductal gray controls brainstem emotional motor systems
700 including respiration. *Prog. Brain Res.* **209**, 379–405.

701 Kittelberger, J.M., Land, B.R., and Bass, A.H. (2006). Midbrain periaqueductal gray and vocal
702 patterning in a teleost fish. *J. Neurophysiol.* **96**, 71–85.

703 Koutsikou, S., Apps, R., and Lumb, B.M. (2017). Top down control of spinal sensorimotor
704 circuits essential for survival. *J. Physiol.* **595**, 4151–4158.

705 Lee, H., Kim, D.-W., Remedios, R., Anthony, T.E., Chang, A., Madisen, L., Zeng, H., and
706 Anderson, D.J. (2014). Scalable control of mounting and attack by Esr1+ neurons in the
707 ventromedial hypothalamus. *Nature* **509**, 627–632.

708 Li, Y., Zeng, J., Zhang, J., Yue, C., Zhong, W., Liu, Z., Feng, Q., and Luo, M. (2018).
709 Hypothalamic Circuits for Predation and Evasion. *Neuron* **97**, 911–924.e5.

710 Lin, D., Boyle, M.P., Dollar, P., Lee, H., Lein, E.S., Perona, P., and Anderson, D.J. (2011).
711 Functional identification of an aggression locus in the mouse hypothalamus. *Nature* **470**, 221–
712 226.

713 Remedios, R., Kennedy, A., Zelikowsky, M., Grewe, B.F., Schnitzer, M.J., and Anderson, D.J.
714 (2017). Social behaviour shapes hypothalamic neural ensemble representations of conspecific
715 sex. *Nature* **550**, 388–392.

716 Schilling, D.L. WILEY SERIES IN TELECOMMUNICATIONS.

717 Shannon, C.E., and Weaver, W. (1964). *The mathematical theory of communication* (Urbana:
718 University of Illinois Press).

719 Smith, B.N., Banfield, B.W., Smeraski, C.A., Wilcox, C.L., Dudek, F.E., Enquist, L.W., and
720 Pickard, G.E. (2000). Pseudorabies virus expressing enhanced green fluorescent protein: A tool

721 for in vitro electrophysiological analysis of transsynaptically labeled neurons in identified central
722 nervous system circuits. *Proc. Natl. Acad. Sci. U. S. A.* 97, 9264–9269.

723 Srivastava, K.H., Holmes, C.M., Vellema, M., Pack, A.R., Elemans, C.P.H., Nemenman, I., and
724 Sober, S.J. (2017). Motor control by precisely timed spike patterns. *Proc. Natl. Acad. Sci. U. S.*
725 *A.* 114, 1171–1176.

726 Stanek, E., 4th, Cheng, S., Takatoh, J., Han, B.-X., and Wang, F. (2014). Monosynaptic
727 premotor circuit tracing reveals neural substrates for oro-motor coordination. *Elife* 3, e02511.

728 Timme, N.M., and Lapish, C. (2018). A Tutorial for Information Theory in Neuroscience. *eNeuro*
729 5.

730 Wang, L., Chen, I.Z., and Lin, D. (2015). Collateral pathways from the ventromedial
731 hypothalamus mediate defensive behaviors. *Neuron* 85, 1344–1358.

732 Wang, L., Talwar, V., Osakada, T., Kuang, A., Guo, Z., Yamaguchi, T., and Lin, D. (2019).
733 Hypothalamic Control of Conspecific Self-Defense. *Cell Rep.* 26, 1747–1758.e5.

734 Yang, C.F., Chiang, M.C., Gray, D.C., Prabhakaran, M., Alvarado, M., Juntti, S.A., Unger, E.K.,
735 Wells, J.A., and Shah, N.M. (2013). Sexually dimorphic neurons in the ventromedial
736 hypothalamus govern mating in both sexes and aggression in males. *Cell* 153, 896–909.

737 Zalcman, S.S., and Siegel, A. (2006). The neurobiology of aggression and rage: role of
738 cytokines. *Brain Behav. Immun.* 20, 507–514.

739

740

Figure 1

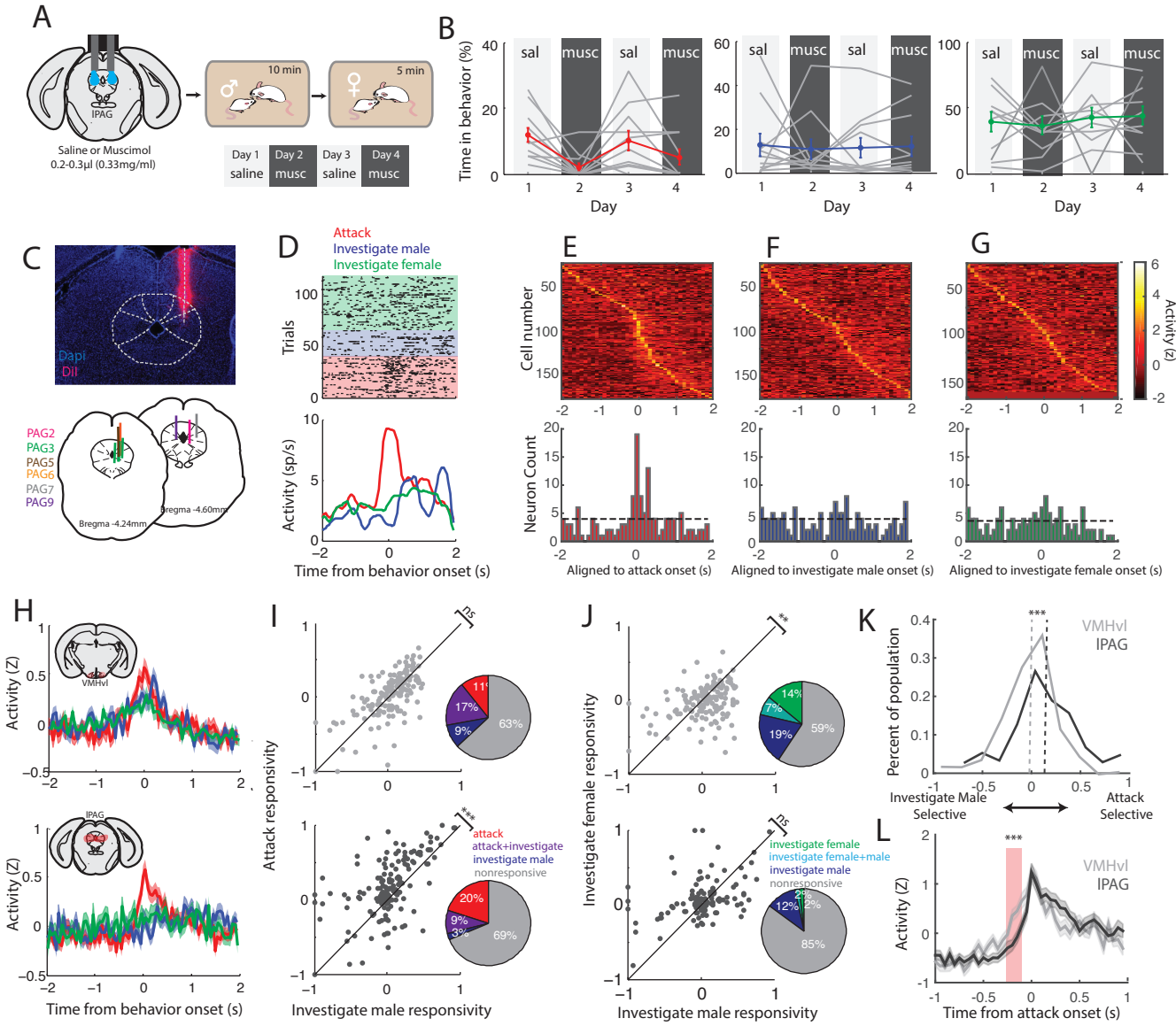


Figure 2

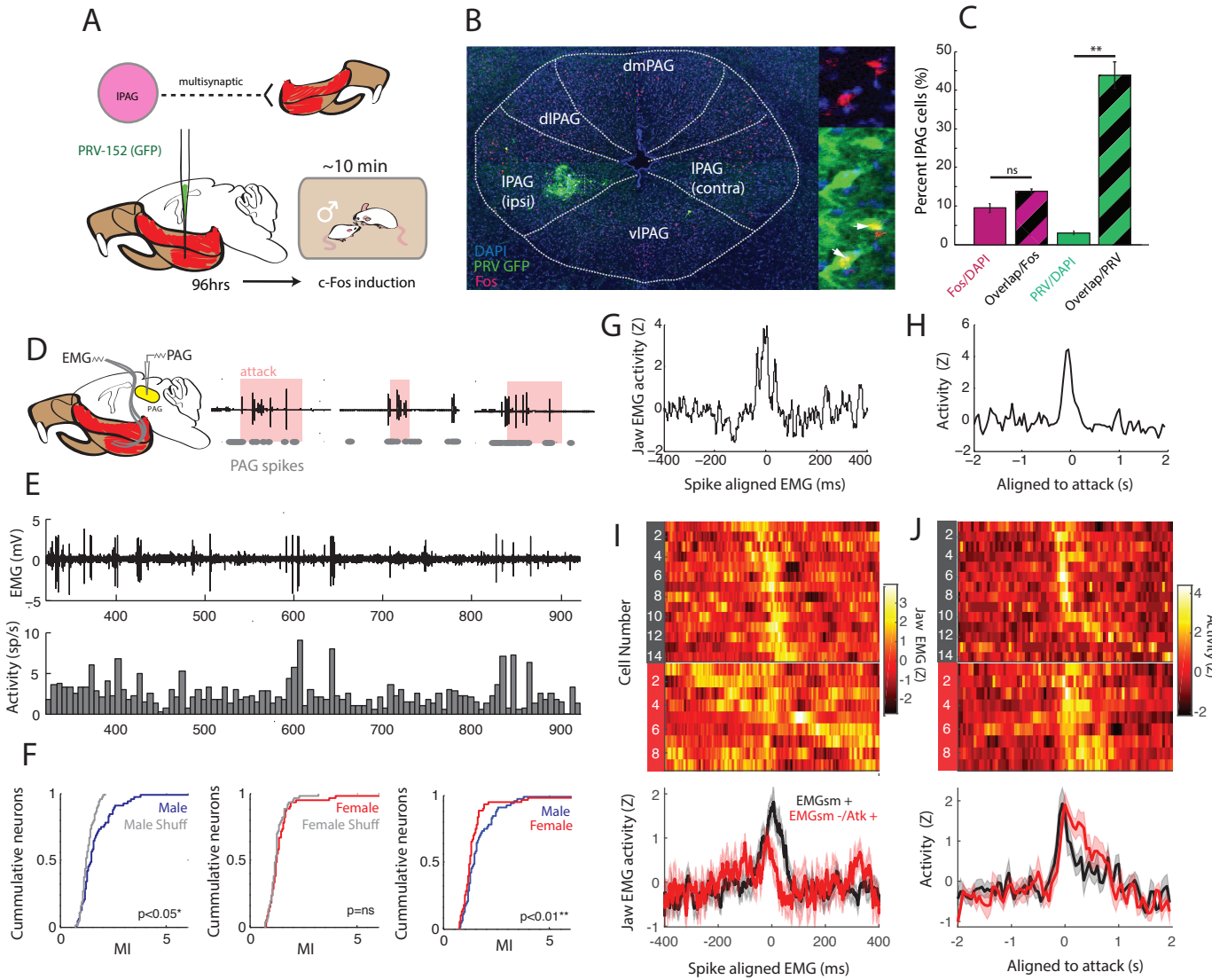
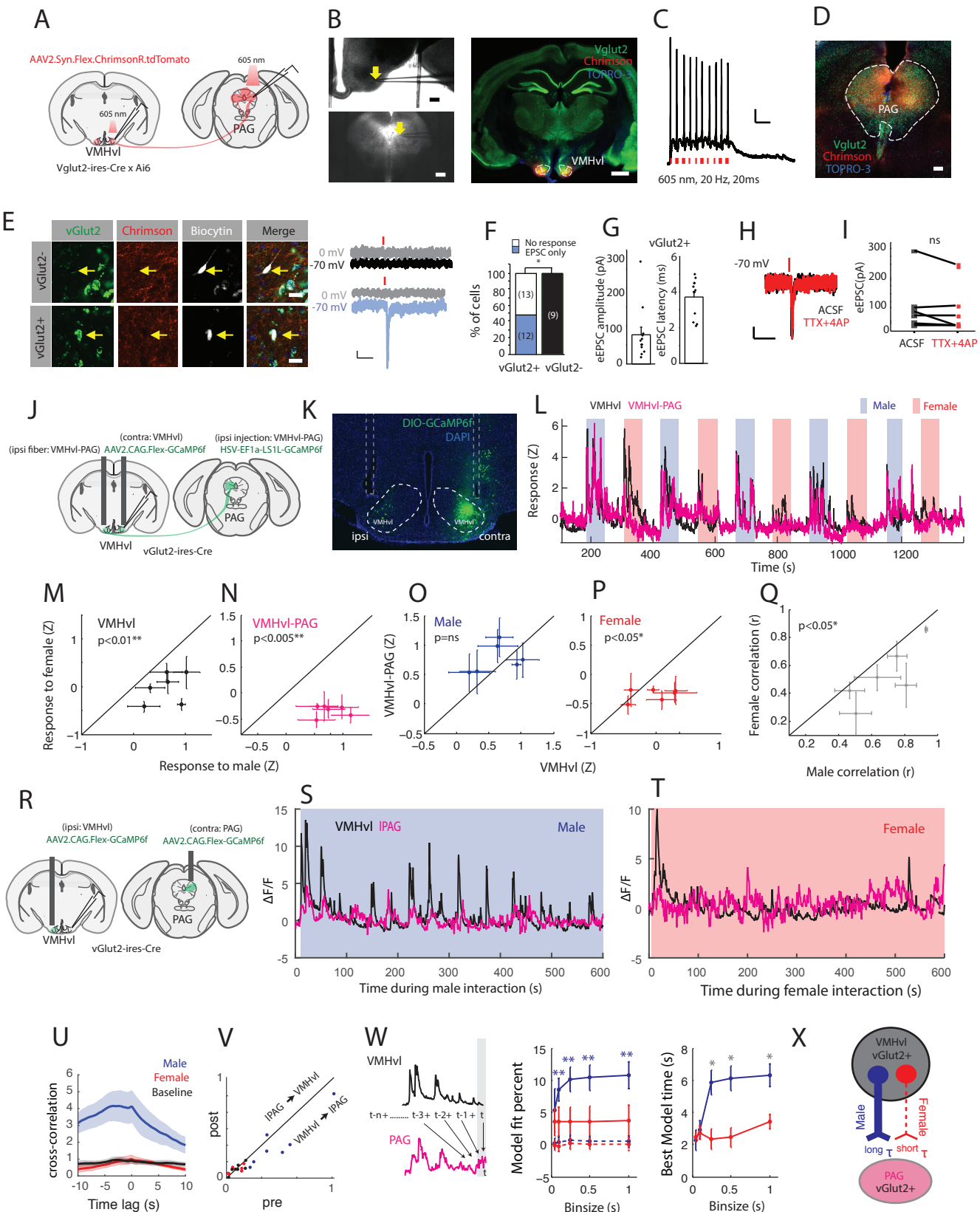
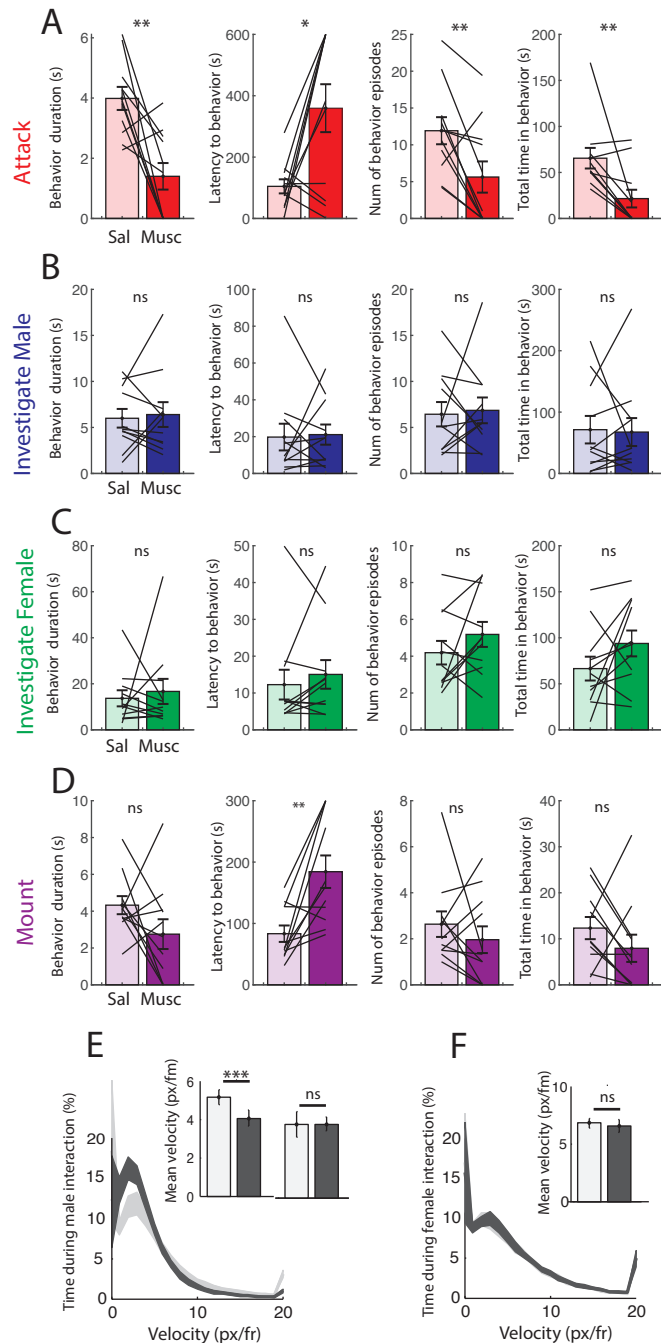


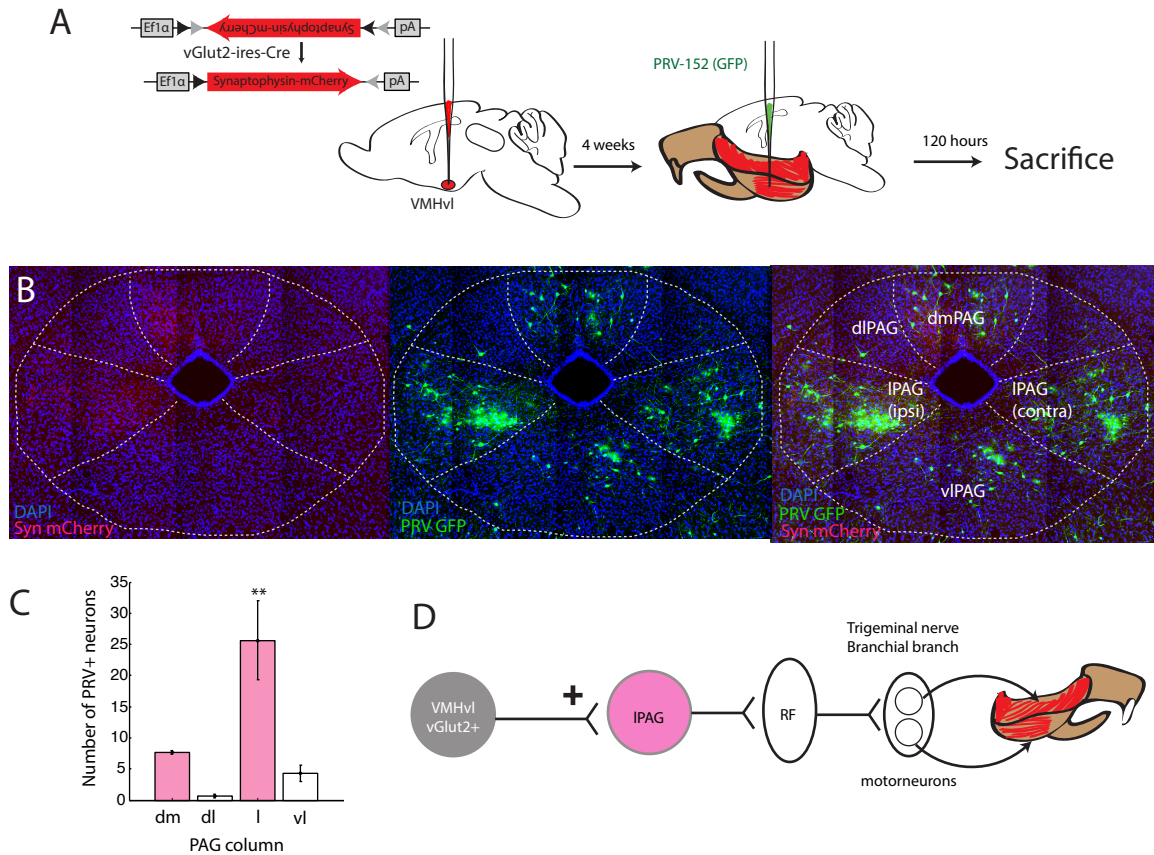
Figure 3



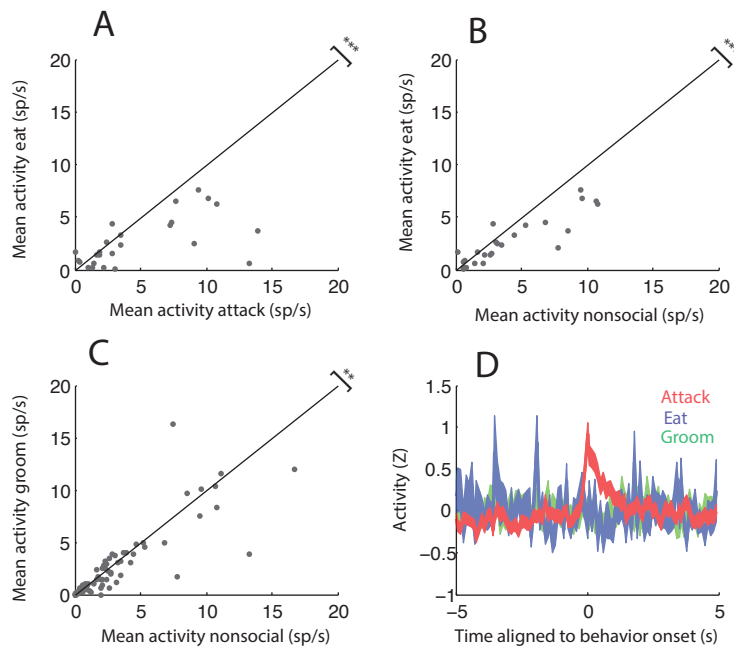
Supplementary Figure 1



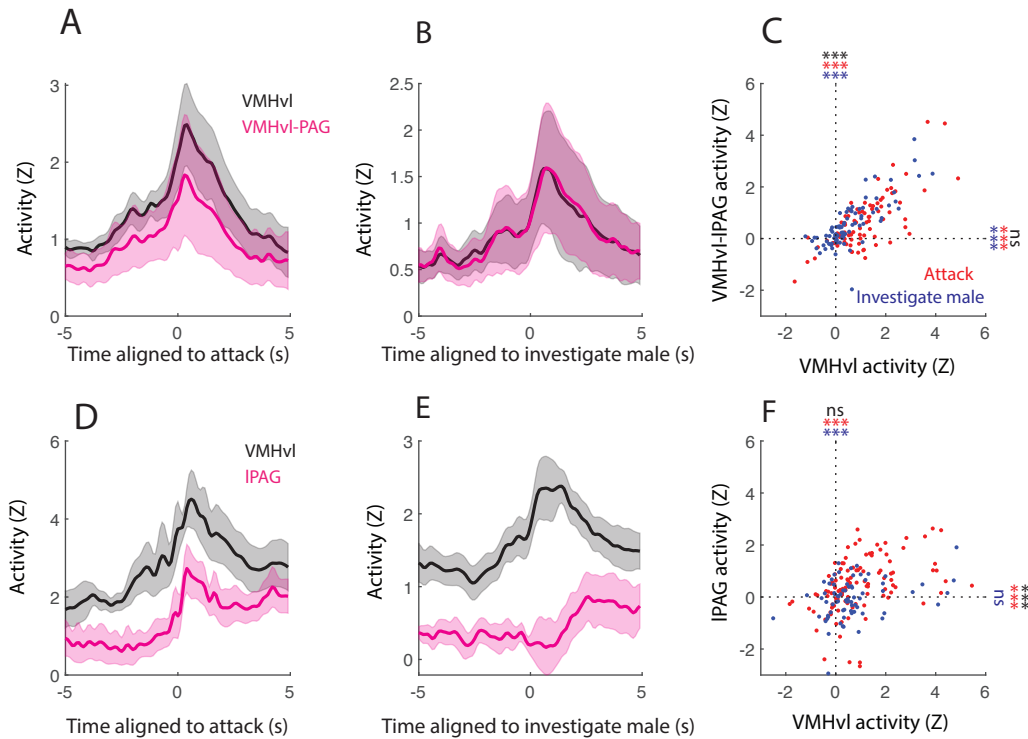
Supplementary Figure 2



Supplementary Figure 3



Supplementary Figure 4



Supplementary Figure 5

